Residual Stress and Distortion Analysis for TMCP Steel Grade EH36 Butt Welding Parts in GTAW-SMAW Hybrid Welding Process using Finite Element Method

Sumeth Nuchim
Department of Mechanical Engineering, Faculty of Engineering, Srinakharinwirot University, Ongkharak, Nakhonnayok, Thailand
sumeth.nuchim@g.swu.ac.th

Phacha Bunyawanichakul
Department of Mechanical Engineering, Faculty of Engineering, Srinakharinwirot University, Ongkharak, Nakhonnayok, Thailand
prachabu@g.swu.ac.th

Natchanun Angsuseranee
Department of Manufacturing Engineering, Faculty of Engineering and Architecture, Rajamangala University of Technology Suvarnabhumi, Phra Nakhon Si Ayutthaya, Thailand
natchanun.a@rmutsb.ac.th (corresponding author)

Visanu Boonmag
Department of Mechanical Engineering, Faculty of Engineering, Thonburi University, Bangkok, Thailand
boonmagvisa@gmail.com

Received: 25 July 2024 | Revised: 6 December 2024, 10 December 2024, and 13 December 2024 | Accepted: 18 December 2024

 DOI: https://doi.org/10.48084/etasr.8506

ABSTRACT

The present work evaluates residual stress and distortion in Thermo-Mechanical Control Process (TMCP) grade EH-36 steel plates subjected to hybrid Gas Tungsten Arc Welding (GTAW) and Shielded Metal Arc Welding (SMAW) processes Specimens measuring 650 × 170 mm with a thickness of 12 mm were utilized. Finite Element Method (FEM) analysis was employed to model residual stress and distortion, a critical step in optimizing the manufacturing process of mechanical structures and parts in shipbuilding. The FE model was developed using ANSYS software incorporating a heat source model with a user-defined subroutine to represent an ellipsoidal moving weld torch with front and rear power density distribution. Heat losses due to radiation and convection were accounted for, while mechanical boundary conditions were applied to restrict rotation and displacement but allow material deformation. Thermal analysis demonstrated close agreement between experimental thermocouple data and numerical simulations, with a temperature deviation of only 5%. Residual stress analysis using X-Ray Diffraction (XRD) revealed that ultrasonic stress relief reduced the maximum residual stress from an average of 193.4 MPa to 39.1 MPa Distortion analysis showed that the maximum FEM deformation was 0.2873 mm, with a 12% deviation from coordinate measuring machine (CMM) results, while the minimum FEM deformation was 0.031922 mm, differing by 3%. The larger deviation occurred in areas with peak distortion, attributed to variations in mechanical restraint positioning, which significantly influence material deformation during cooling.

Keywords-residual stress; distortion; EH36 steel; GTAW-SMAW; hybrid welding; FEM

I. INTRODUCTION

The demand for heavy, thick plates with an optimal combination of high strength, toughness, and weldability has significantly increased in recent years, especially for constructing large container ships. The successful application of Thermo-Mechanical Control Process (TMCP), coupled with recent technological innovations, has led to the development of EH36, EH40, and EH47 grade steel plates. For EH36 steel plates, high heat input welding has been successfully developed, ensuring good toughness in the Heat-Affected Zone (HAZ) by enhancing the thermal stability of TIN particles at elevated temperatures. This high-strength steel is extensively utilized in structural components across the shipbuilding, oil and gas industries[1]. Welding is a widely used joining technique used in engineering due to its advantages in design flexibility, cost-effectiveness, and weight reduction. Over the years, several welding techniques have been developed, with ongoing advancements attracting interest across various industrial sectors [2]. Gas Tungsten Arc Welding (GTAW), also known as Tungsten Inert Gas (TIG) welding, is recognized for its high controllability and cost-efficient equipment, making it ideal for precision welding of thin sheets. This process is applicable to a wide range of materials [3, 4]. Conversely, Shielded Metal Arc Welding (SMAW) is commonly employed for EH36 steel plates because of its simplicity, affordability, and portability [5]. In the shipbuilding industry, the welding methodology for TMCP-grade EH36 hull shell plates have transitioned from relying solely on SMAW to a hybrid GTAW-SMAW approach. In this hybrid process, the GTAW method is used for root passes, while subsequent passes are completed using SMAW. This approach combines the quality advantages of both welding techniques [6]. Metals experience changes in mechanical and physical properties due to the thermal cycle during welding. As the weld area heats up, the material's yield strength and elastic modulus decrease, while specific heat capacity and thermal expansion increase. These changes contribute to material shrinkage, deformation, and variations in heat flow and distribution uniformity [7]. Residual stresses in welded joints significantly influence the occurrence of fatigue failure, brittle fractures, and hot cracking in the weld zone. Additionally, residual stresses can initiate and propagate cold cracks and fatigue cracks under ambient conditions. Corrosion cracking in residual stress regions may also lead to the rapid failure of weld joints in corrosive environments [8]. Consequently, analyzing residual stress is a crucial step in designing and manufacturing components, as it helps evaluate their reliability under various loading conditions.

Numerical simulation using Finite Element Methods (FEM) is a widely accepted technique for predicting and analyzing welding-induced residual stresses. FEM offers advantages such as reduced time, lower costs, and enhanced versatility compared to experimental measurements [9]. Goldak's ellipsoidal heat source model has been extensively applied in numerical simulations to predict residual stresses and distortions caused by transient thermal fields during welding. Studies have shown that these simulations provide results in good agreement with experimental validations [10].

Several studies have focused on analyzing the thermal effects, residual stresses, and distortions associated with welding joints. Authors in [11] examined residual stress and distortion caused by metal active gas welding of S355JR steel using FEM, with experimental results showing good agreement with simulations. In [12], researchers analyzed the residual stress and thermal field for SMAW of SA738GR.B thick plates using FE with Goldak's ellipsoid heat source model, achieving stress field validation within 12.5% error. Studies in [13] focused on residual stress and deformation induced by two-pass TIG welding of Al 2219 plates, with experimental validation showing average errors of 18.8% for stress and 17.4% for deformation. Additionally, in [14] authors examined the impact of porosity on residual stress and thermal analysis in aluminum alloy 2024 butt joints using Finite Element Analysis (FEA) and 3D Computed Tomography (GT). Authors in [15] modeled welding-induced distortions in ultra-high strength steel S960 MC, incorporating thermal and solid-state phase transformations in ABAQUS. From the results of the mechanical simulations and comparison with measured deformations, it is observable that a more accurate prediction of welding-induced angular and bending distortions is possible when the effect of SSPT is incorporated for the material under investigation. In [16], investigations analyzed thermal and residual stress fields TWIP-Ti steel through the GTAW process. A FE thermo-mechanical model was employed to analyze the welding thermal cycle in the TWIP-Ti steel while the numerical prediction of residual stress was validated by X-Ray Diffraction (XRD) measurements in welding critical regions. The results provided good weldability of the TWIP-Ti steel in higher plate thickness through the GTAW process at low heat input. Studies in [17] predicted distortions and residual stresses in thick plate weld joint of austenitic stainless steel through the GTAW process. The differences in numerical and experimental results for maximum temperature, maximum distortion, and longitudinal and transverse residual stresses were 4.5%, 2.61%, 23.5%, and 5.23%, respectively. Distortions predicted using isotropic material hardening model were closer to experiments compared to that predicted using the kinematic material hardening model. In [18], researchers explored thermal, residual stress and distortion in dissimilar T-joints using SMAW. Authors in [19] studied thermal and residual stress distributions in Inconel 625 welded using GTAW, validated by XRD. The thermal measurements were collected bypass from the analysis, and the agreement was 9.08%. The agreement between the measured and analyses residual stress was 11%. Finally, in [20] authors examined the effects of hybrid GTAW-SMAW parameters on weld HAZ hardness in low carbon steel. The results demonstrate that weld hardness was affected by GTAW current whereas SMAW current affected the HAZ hardness.

The objective of this study is to investigate the residual stresses and distortions induced in EH36 steel during multi-pass welding employing a hybrid GTAW-SMAW process. The study examines welded beads and surrounding regions subjected to plastic deformation due to thermal cycling. Thermal and lattice spacing variations affecting microstructure and thermomechanical stresses in the weldment are analyzed. Using FEM, the study aims to forecast the degree of thermal

influence on the weldment. Since no prior research has examined the thermal behavior of GTAW-SMAW hybrid welding for EH36 steel, this study addresses the lack of confirmatory simulations for temperature profiles and residual stress estimations. The thermomechanical analysis is conducted in 3D using ANSYS, with thermocouples measuring welding temperatures and X-ray diffraction evaluating residual stress in cooled weldments for verification.

II. MATERIALS AND METHODS

A. Welding Procedure

GTAW and SMAW processes were employed on EH36 steel plates. The chemical composition of the base metal is presented in Table I. Welding was performed using filler materials that matched the base metal's properties. For GTAW, AWS A5.18 ER 70S-6 filler material was utilized, with its composition detailed in Table II. For SMAW, AWS A5.1 E7016 filler material was used, with its chemical composition outlined in Table III.

The welded joint geometry consisted of two plates joined with a V-groove configuration, with dimensions and details illustrated in Figure 1. The hybrid welding procedure, integrating GTAW for the root pass and SMAW for subsequent passes, was carried out following the parameters specified in Tables IV and V, respectively. Figure 2 depicts the hybrid welding process using GTAW and SMAW according to AWS D1.1 standards.

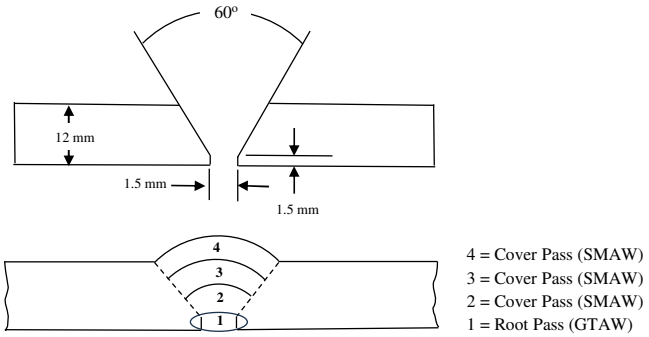

Fig. 1. Dimensions of steel two plates and hybrid welding procedure.

TABLE I. CHEMICAL COMPOSITION OF EH36 STEEL

Grade	EH36 (%wt)
C	0.144
Si	0.326
Mn	1.40
P	0.0152
S	0.0067
Nb	0.027
V	0.024
Mo	0.006
Cr	< 0.005
Cu	0.01
Ti	0.011
Ni	0.006
Al	0.047

TABLE II. CHEMICAL COMPOSITION OF AWS A5.18 ER 70S-6 [21]

Filler metal	AWS A5.18 ER 70S-6 (%wt)
C	0.04
Si	0.85
Mn	1.46
P	0.012
S	0.014
Cu	0.11
Cr	0.02
Ni	0.01
Mo	0.01
V	0.01

TABLE III. CHEMICAL COMPOSITION OF AWS A5.1 E7016 [22]

Filler metal	AWS A5.1 E7016 (%wt)
C	0.08
Si	0.64
Mn	0.86
P	0.012
S	0.008

TABLE IV. WELDING PARAMETERS OF GTAW

Parameters	GTAW
Electrode type	AWS A5.18 ER 70S-6
Electrode diameter	2.4 mm
Current intensity	120 A
Welding speed	59.1667 mm/min
Shielding gas flow volume	16 liters/min

TABLE V. WELDING PARAMETERS OF SMAW

Parameters	SMAW
Electrode type	AWS A5.1 E7016
Electrode diameter	3.2 mm
Current intensity	120 A
Welding speed-cover pass 2	46.43 mm/min
Welding speed-cover pass 3	32.50 mm/min
Welding speed-cover pass 4	38.23 mm/min

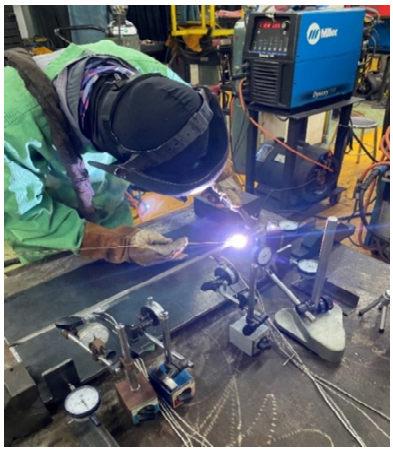

Fig. 2. GTAW-SMAW hybrid welding process.

B. Thermal Analysis

The temperature during the welding process was monitored using several K-type thermocouples attached to the side surfaces of the parent material. Eight thermocouples were

strategically positioned along the weld centerline to measure temperature variations, as schematically illustrated in Figure 3.

The thermal simulation of the EH36 steel butt-weld joint was conducted using a three-dimensional model, as shown in Figure 4. The plate dimensions were 650 mm x 170 mm with a thickness of 12 mm. The model's coordinate system and mesh divisions are depicted in Figure 5. The mesh consisted of a defined number of elements and nodes. To ensure accuracy and minimize error, numerical simulations were performed three times with varying numbers of elements, ultimately selecting the configuration that yielded the least error values. Due to the symmetry of the weld sample, only half of the welding section was analyzed, taking the weld centerline as the axis of symmetry. Heat transfer data from the simulation was extracted at four different positions -T_1, T_2, T_3 and T_4- on the weld model, measured at time interval of 150 and 450 seconds. These positions included the heat source location at the weld centerline at distances of 9 mm, 15 mm, 35 mm, and 105 mm away from the centerline, as detailed in Figure 6.

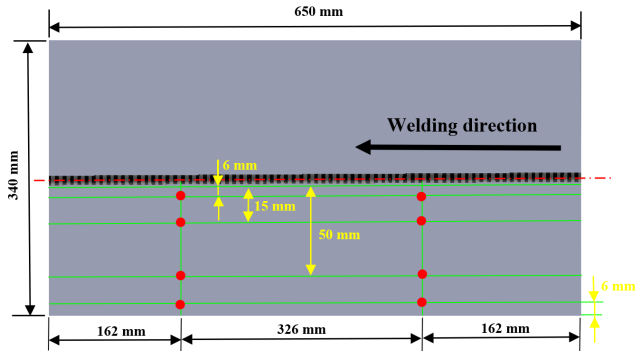

Fig. 3. Positions of eight thermocouples on the surface of the workpiece.

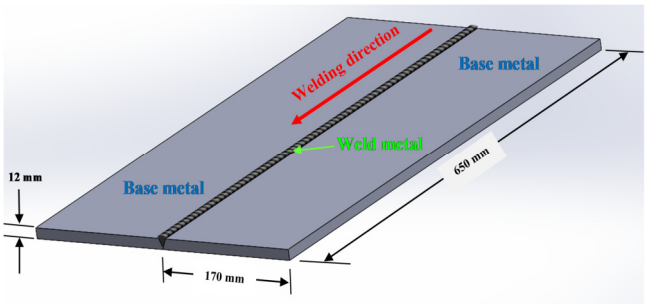

Fig. 4. Three-dimensional model of the EH36 steel butt-weld joint.

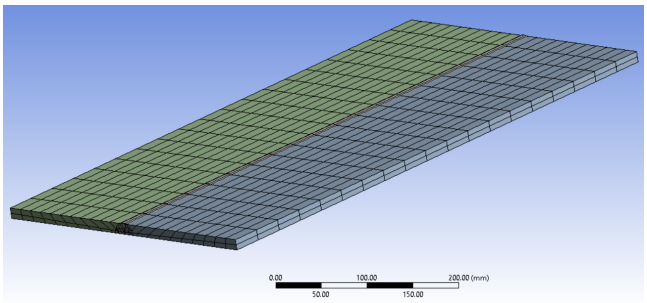

Fig. 5. Mesh obtained from numerical simulations.

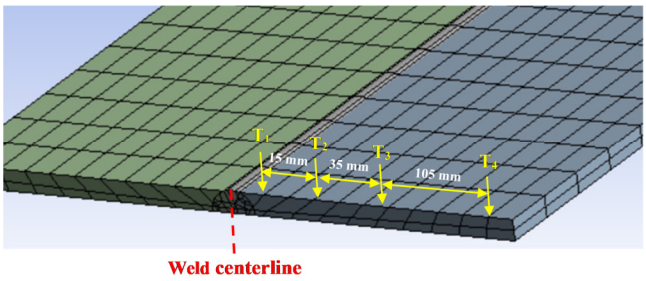

Fig. 6. Heat transfer position.

C. Residual Stress Analysis

Residual stresses induced by the weld thermal cycle were experimentally analyzed and compared with the results from FEM to validate the FE model. Stress measurements were performed using an X-ray diffractometer (model: XSTRESS 3000). The parameters for the diffractometer are provided in Table VI. Figure 7 illustrates the residual stress measurement, which is capable of examining only near-surface stresses. Consequently, the comparison between experimental and FEM results was restricted to surface stresses. Measurements were taken in 5 mm intervals along the transverse direction and 30 mm intervals along the longitudinal direction of the weld bead.

TABLE VI. XRD MEASUREMENT PARAMETERS

X-ray Diffraction Parameters	Specification/Values
Tube type	Cr
Max. Current	9 A
Max. Power	270 W
Supplied current during the experiment	6.7 A
Supplied voltage during the experiment	30 V
Exposure time for the calibration	8 s
Exposure time for measurement	10 s
Collimator diameter	3 mm
Collimator distance	10.390 mm
Detector distance	50 mm
Tilt angle	0° to 45°
Number of tilts	5/5
Rotation angle	0° to 90°
Number of rotations	2

Fig. 7. Residual stress measurement using XRD.

The FEM was developed using ANSYS simulation software to predict residual stresses resulting from the hybrid GTAW-SMAW welding of EH36 steel plate butt joints. The model employed a double-ellipsoid heat source to simulate the heat distribution on the welding surface. Heat flux transferred sequentially from the surface of one element to the next, following the welding path, using the birth-and-death technique

to simulate material deposition during the welding process. The simulation assumed that residual stress is primarily influenced by the reduction in the cross-sectional area of the weld. FEMs are essential to capture the coupling effects between thermal histories, elastic properties at high temperatures, and residual stress of the consequent development. The model was adapted to a practical square butt weld configuration to reflect real-world applications. Detailed validation was conducted to ensure the reliability and accuracy of the process model.

D. Experimental Distortion

Distortion measurements were conducted using a Coordinate Measuring Machine (CMM). The deformation induced on the weld plate was recorded using a three-dimensional CMM (Mitutoyo: Beyond-A910). Measurements were taken both before and after welding. Nine specific points were selected from each section of the plate along the transverse direction, with measurements performed at 10 mm intervals. The displacements along the z-axis were recorded, and the experimental results of the induced deformation are illustrated in Figure 8.

For the distortion simulation, ANSYS was utilized with the same material shape and element divisions as those used in the temperature distribution analysis. The simulation modeled two EH36 structural steel plates, each with dimensions of 650 mm × 170 mm × 12 mm, joined using hybrid GTAW-SMAW butt welding. The material properties of the base metal include a yield strength of 355 MPa and a tensile strength of 490–620 MPa at room temperature [21].

Fig. 8. Experimental measurement welding distortion.

III. RESULTS AND DISCUSSIONS

A. Thermal Analysis

Temperature measurements during the welding process, recorded using thermocouples, were as follows: Position T_1 reached 1225 ^oC, Position T_2 recorded 965 ^oC, Position T_3 measured 696 ^oC, and Position T_4 showed 156 ^oC.

Figure 9 illustrates the results of the thermal simulation, depicting the temperature distribution on the plate from the numerical simulation performed three times. Temperature at Position T_1, located at the weld centerline, reached a peak of 1174.1 °C. Uneven cooling due to convection and radiation caused a rapid decrease in temperature after the heat source moved past the location. For the subsequent positions, temperatures were recorded as 917.97 ^oC at T_2, 661.81 ^oC at T_3, and 149.49 ^oC at T_4. The heat generated during welding was transferred to the lower-temperature regions of the plate by conduction, while heat was dissipated into the environment through radiation and convection.

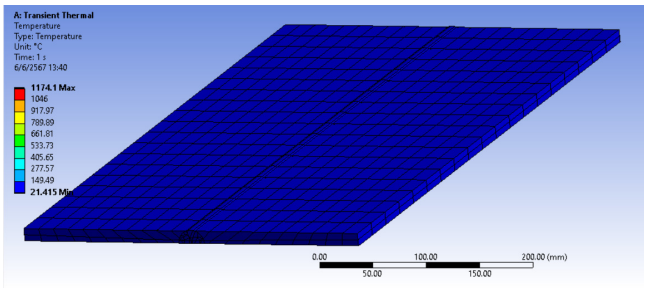

Fig. 9. Temperature distribution obtained from numerical simualtions.

B. Residual Stress Analysis

Figure 10 illustrates the results of the numerical simulation of residual stress for EH36 steel.

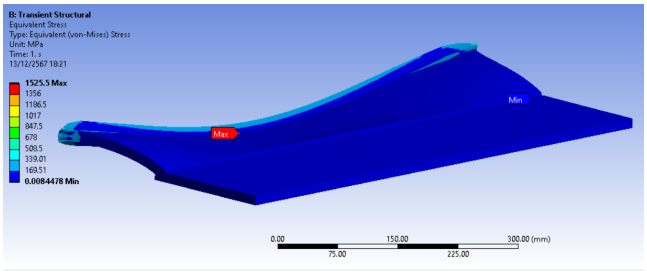

Fig. 10. Residual stress EH36 steel simulation.

The centerline of the weld at 0 mm corresponds to the HAZ, a region experiencing high temperatures during welding but not sufficient to cause melting. This undergoes rapid cooling. The tensile residual stress measured for EH36 steel at the weld centerline is 169.51 MPa. By comparison, the XRD measurements provide a tensile residual stress of 193.4 ± 26.1 MPa. The values are consistent, with a difference of approximately 14%. At a distance of 10 mm from the weld centerline, near the HAZ, the FEA simulation records a comprehensive residual stress of -112.76 MPa, while the XRD measurements provide a compressive residual stress of −116.8 ± 9.8 MPa. These results are consistent, with a difference of about 4%. At 30 mm from the weld centerline, the FEA value shows a tensile residual stress of 37.5 MPa. In comparison, the tolerance range measured by XRD reports a tensile residual stress of 39.1 ± 17.5 MPa. These values are also consistent, with a difference of approximately 4%. In conclusion, the comparison between the simulated and measured residual stress values demonstrates good agreement. The differences are within acceptable limits, confirming the reliability of the (FEA model for predicting residual stresses in hybrid GTAW-SMAW welding of EH36 steel.

Figure 11 compares the residual stress measured by XRD with the residual stress predicted by the FEM. The results

indicate that residual stress in the longitudinal direction was tensile (positive) at 0 mm from the middle of the weld beads. Additionally, the longitudinal residual stress remained predominantly tensile in regions near the weld beads. This tensile residual stress is a critical factor, as it often contributes to the initiation of fatigue cracks in the material.

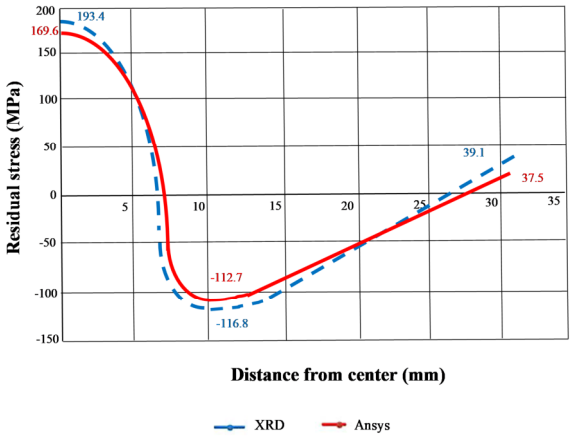

Fig. 11. Residual stresses in the transverse direction.

C. *Comparison Between FEM and Experimental Distortion*

As the heat source moves along the weld centerline, the material experiences plastic deformation and shrinkage due to a gradual, non-uniform temperature drop. During the cooling phase, the continuous temperature decrease causes the hot base material and HAZ to shrink. At a certain point, the material's strength increases as the temperature drops further, creating resistance to shrinkage. Consequently, the weld plate remains in a strained state due to the contraction behavior.

Material shrinkage during cooling is significantly affected by the variation in thermal expansion between the weld zone and the lower-temperature base metal. This interaction drives the distortion observed in the weldment. The FE analysis of welding deformation induced along the longitudinal and transverse directions is shown in Figure 12. The highest deformation along the z-axis recorded by experimental measurement and FEM simulation was 0.2873 mm and 0.031922 mm, respectively, both occurring around the weld zone.

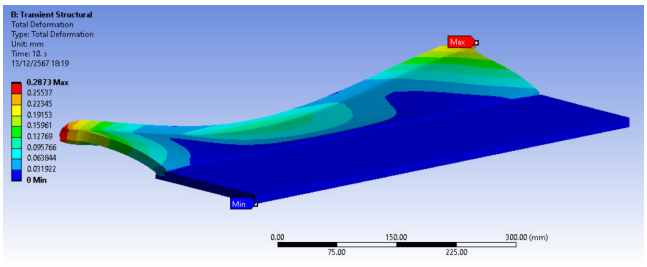

Fig. 12. FE welding deformation.

The results are compared in Figure 13, where the variations between experimental and FEM data ranged from 3% to 12%. The largest deviation of 12% was observed in the region of peak distortion. This discrepancy is attributed to differences in the mechanical restraint positioning, which plays a crucial role in resisting material deformation during the cooling phase of welding. The observed distortion has practical implications, as it may necessitate repair and rework, reducing the aesthetic value of the workpiece and increasing manufacturing costs.

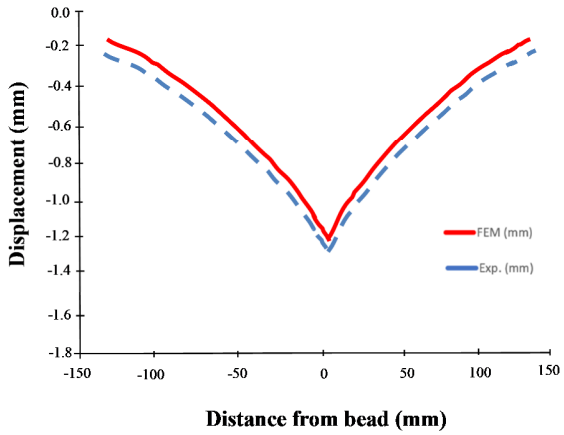

Fig. 13. The evaluated positions near the weld zone and plate edges, illustrating the resulting angular distortion on both sides of the plate (Sides A and B).

Figure 14 illustrates the process for computing angular distortion. y_i represents the measured z-displacement at the edge, l_i is the distance between the point measured near the weld (P_i) and the edge point (R_i), and x_i denotes half the width of the plate. The resulting angular distortion, θ_i, is calculated for each side, identified as a and b Therefore, the angular distortion can be determined by:

$$\theta_i = sin^{-1}\left(\frac{y_i}{l_i}\right) \quad (1)$$

where $i = a, b$. The distance l_i is 174 mm and the calculated angular distortions for both sides of the plate are $\theta_a = 0.41^o$ and $\theta_b = 0.41^o$, respectively.

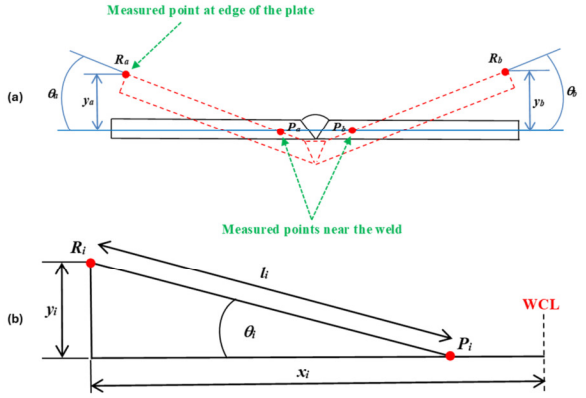

Fig. 14. Computation of angular distortion: (a) distorted weld metal geometry and (b) measured locations to determine the corresponding angular distortion values.

IV. CONCLUSIONS

This study investigated the thermal behavior, residual stresses, and deformation characteristics of hybrid Gas Tungsten Arc Welding- Shield Metal Arc Welding (GTAW-SMAW) welding on EH36 steel plates. The following conclusions were drawn:

- **Thermal Analysis**: The accuracy of the temperature measurements using thermocouples and numerical simulations was validated, with temperature values differing by no more than 5%. The rapid cooling effect, driven by convection and radiation, caused a steep temperature gradient. Heat accumulated in the weld zone was transferred to cooler regions via conduction and dissipated into the surrounding environment through radiation and convection.
- **Residual Stress Analysis**: X-Ray Diffraction (XRD) measurements demonstrated that ultrasonic stress relief significantly reduced residual stress in the welded sample. The maximum residual stress before stress relief was 193.4 MPa, which decreased to 39.1 MPa post-treatment. These results confirm the effectiveness of ultrasonic stress relief in mitigating welding-induced residual stresses.
- **Distortion Analysis**: Experimental distortion measurements revealed a maximum FEM deformation of 0.2873 mm., showing a 12% deviation from coordinate measuring machine (CMM) results in areas of peak distortion. The minimum Finite Element Model (FEM) deformation of 0.031922 mm exhibited only a 3% difference from CMM measurements. The larger deviations were attributed to variations in mechanical restraint positioning, which significantly influences material deformation during cooling.
- **Impact of Material Properties**: Distortion and residual stress were found to depend on the relative strength of the weld and base materials. Angular distortion and longitudinal residual stresses were higher for welds with increased strength relative to the base material. This effect was particularly pronounced across the material's thickness.

ACKNOWLEDGMENT

This research was supported by the Department of Mechanical Engineering, Faculty of Engineering, Srinakharinwirot University of Technology for research equipment and facilities. The authors express thanks to the National Metal and Materials Technology Center (MTEC) for providing help and guidance on experiments and simulations.

REFERENCES

[1] K.-K. Um, S.-H. Kim, K.-B. Kang, Y.-H. Park, and O. Kwon, "High Performance Steel Plates For Shipbuilding Applications," presented at the The Eighteenth International Offshore and Polar Engineering Conference, Jul. 2008.

[2] F. Caiazzo *et al.*, "Laser Beam Welding of a Ti–6Al–4V Support Flange for Buy-to-Fly Reduction," *Metals*, vol. 7, no. 5, May 2017, Art. no. 183, https://doi.org/10.3390/met7050183.

[3] V. M. J. Varghese, M. R. Suresh, and D. S. Kumar, "Recent developments in modeling of heat transfer during TIG welding—a review," *The International Journal of Advanced Manufacturing Technology*, vol. 64, no. 5, pp. 749–754, Feb. 2013, https://doi.org/10.1007/s00170-012-4048-9.

[4] V. Msomi and S. Mabuwa, "Analyzing the Influence of Microstructure on the Mechanical Properties of TIG Welded Joints processed by Friction Stir considering the sampling Orientation," *Engineering, Technology & Applied Science Research*, vol. 14, no. 1, pp. 12470–12475, Feb. 2024, https://doi.org/10.48084/etasr.6459.

[5] I. P. Wardani, V. A. Setyowati, S. Suheni, and I. P. Samudra, "The Effect of Welding Current on AISI 1045 Strength and Corrosion Rate," *Journal of Applied Sciences, Management and Engineering Technology*, vol. 1, no. 2, pp. 40–45, Nov. 2020, https://doi.org/10.31284/j.jasmet.2020.v1i2.1159.

[6] A. Jayant and M. S. Dhillon, "Use of analytic hierarchy process (AHP) to select welding process in high pressure vessel manufacturing environment," *International Journal of Applied Engineering Research*, vol. 10, no. 8, pp. 586–595, 2015.

[7] D. Deng, H. Murakawa, and W. Liang, "Prediction of welding distortion in a curved plate structure by means of elastic finite element method," *Journal of Materials Processing Technology*, vol. 203, no. 1, pp. 252–266, Jul. 2008, https://doi.org/10.1016/j.jmatprotec.2007.10.009.

[8] Y. H. P. Manurung *et al.*, "Welding distortion analysis of multipass joint combination with different sequences using 3D FEM and experiment," *International Journal of Pressure Vessels and Piping*, vol. 111–112, pp. 89–98, Nov. 2013, https://doi.org/10.1016/j.ijpvp.2013.05.002.

[9] H. W. Ahmad, J. H. Hwang, J. H. Lee, and D. H. Bae, "Welding Residual Stress Analysis and Fatigue Strength Assessment of Multi-Pass Dissimilar Material Welded Joint between Alloy 617 and 12Cr Steel," *Metals*, vol. 8, no. 1, Jan. 2018, Art. no. 21, https://doi.org/10.3390/met8010021.

[10] O. Obeid, G. Alfano, H. Bahai, and H. Jouhara, "Numerical simulation of thermal and residual stress fields induced by lined pipe welding," *Thermal Science and Engineering Progress*, vol. 5, pp. 1–14, Mar. 2018, https://doi.org/10.1016/j.tsep.2017.10.005.

[11] Y. Rong, G. Zhang, and Y. Huang, "Study of Welding Distortion and Residual Stress Considering Nonlinear Yield Stress Curves and Multi-constraint Equations," *Journal of Materials Engineering and Performance*, vol. 25, no. 10, pp. 4484–4494, Oct. 2016, https://doi.org/10.1007/s11665-016-2259-1.

[12] X. Yang *et al.*, "Welding Temperature Distribution and Residual Stresses in Thick Welded Plates of SA738Gr.B Through Experimental Measurements and Finite Element Analysis," *Materials*, vol. 12, no. 15, Jan. 2019, Art. no. 2436, https://doi.org/10.3390/ma12152436.

[13] A. S. Ahmad, Y. Wu, H. Gong, and L. Nie, "Finite Element Prediction of Residual Stress and Deformation Induced by Double-Pass TIG Welding of Al 2219 Plate," *Materials*, vol. 12, no. 14, Jan. 2019, Art. no. 2251, https://doi.org/10.3390/ma12142251.

[14] P. Poolperm, W. Nakkiew, and N. Naksuk, "Finite element analysis of the effect of porosity on residual stress in 2024 aluminium alloy GTAW," *Materials Research Express*, vol. 7, no. 5, Feb. 2020, Art. no. 056518, https://doi.org/10.1088/2053-1591/ab906a.

[15] M. Ghafouri, J. Ahn, J. Mourujärvi, T. Björk, and J. Larkiola, "Finite element simulation of welding distortions in ultra-high strength steel S960 MC including comprehensive thermal and solid-state phase transformation models," *Engineering Structures*, vol. 219, Sep. 2020, Art. no. 110804, https://doi.org/10.1016/j.engstruct.2020.110804.

[16] V. García-García, I. Mejía, F. Reyes-Calderón, J. A. Benito, and J. M. Cabrera, "FE thermo-mechanical simulation of welding residual stresses and distortion in Ti-containing TWIP steel through GTAW process," *Journal of Manufacturing Processes*, vol. 59, pp. 801–815, Nov. 2020, https://doi.org/10.1016/j.jmapro.2020.09.042.

[17] S. D. Banik, S. Kumar, P. K. Singh, S. Bhattacharya, and M. M. Mahapatra, "Distortion and residual stresses in thick plate weld joint of austenitic stainless steel: Experiments and analysis," *Journal of Materials Processing Technology*, vol. 289, Mar. 2021, Art. no. 116944, https://doi.org/10.1016/j.jmatprotec.2020.116944.

[18] R. Sepe, V. Giannella, A. Greco, and A. De Luca, "FEM Simulation and Experimental Tests on the SMAW Welding of a Dissimilar T-Joint," *Metals*, vol. 11, no. 7, Jul. 2021, Art. no. 1016, https://doi.org/10.3390/met11071016.

[19] H. Vemanaboina, E. Gundabattini, K. Kumar, P. Ferro, and B. Sridhar Babu, "Thermal and Residual Stress Distributions in Inconel 625 Butt-Welded Plates: Simulation and Experimental Validation," *Advances in Materials Science and Engineering*, vol. 2021, no. 1, 2021, Art. no. 3948129, https://doi.org/10.1155/2021/3948129.

[20] P. P. Thakur and A. N. Chapgaon, "Effect of GTAW-SMAW hybrid welding process parameters on hardness of weld," *Gas*, vol. 100, no. 110, 2017, Art. no. 120.

[21] "China AWS A5.18 ER70S-6 Carbon Steel Welding Wire Filler Metals for Gas Shielded Arc Welding, Solid Wires Manufacturer and Supplier | Tianyu," TYUE. https://www.tyueweld.com/aws-a5-18-er70s-6-carbon-steel-filler-metals-for-gas-shielded-arc-welding-product/.

[22] "Electric welding wire KOBE LB-52U." ARC Welding Service CO.,LTD. https://www.arcweldingservice.com/product/product_detail/1524.